Cement and Concrete Research 42 (2012) 643–655

Contents lists available at SciVerse ScienceDirect

Cement and Concrete Research

journal homepage: http://ees.elsevier.com/CEMCON/default.asp

An experimental study on the bond strength between reinforcement bars and concrete as a function of concrete cover, strength and corrosion level

Hakan Yalciner, Ozgur Eren *, Serhan Sensoy

Department of Civil Engineering, Eastern Mediterranean University, Gazimagusa, Mersin 10, Turkey

ARTICLE INFO

Article history:
Received 17 May 2011
Accepted 27 January 2012

Keywords:
Corrosion (C)
Pullout test (C)
Bond strength (C)
Bond-slip (C)

ABSTRACT

The effect of corrosion on the bond strength between reinforcement bars and concrete was studied in a series of experiments. An accelerated corrosion method was used to corrode the reinforcement bars embedded in concrete specimens. Pullout tests were performed to develop an empirical model for the ultimate bond strength by evaluating bond strengths in two different concrete mixes, three concrete cover depths and different mass losses of reinforcement bars after corrosion. Bond-slip relationships for the different corrosion levels were compared. It was found that the relationship between bond strength and concrete strength in uncorroded specimens differed from that of corroded specimens set in high-strength concrete because of brittleness in the corroded specimens, which caused a sudden loss of bond strength. The results revealed that specimens with higher concrete strength levels and corroded reinforcements showed a higher percentage of bond strength degradation due to concrete cracking during the pullout tests.

1. Introduction

The corrosion of reinforcement bars embedded in concrete is regarded as the most important factor in the deterioration of concrete structures and can lead to serious damage [1]. Due to the economic impact and effects on the service life of reinforced concrete structures caused by corrosion, the durability of concrete and the bond strength between reinforcement bars and concrete has remained a popular research subject of serious academic interest. In previous works, a series of bond strength models has been developed in attempts to predict the remaining service life of these structures. For instance, two bond strength models were developed by Cabrera [2]: one for regular Portland cement concrete and the other for fly ash concrete. Cabrera [2], in his study, used a concrete mixture with a water-cement ratio (w/c) of 0.55. The 28-day compressive strength of the concrete was not reported. The corrosion percentage was varied from 0% (for the control specimens) up to 12.6%. Another experimental study was conducted by Auyeung et al. [3] with the aim of predicting bond strength as a function of mass loss due to the corrosion of the reinforcing bars, where a concrete mixture with a w/c ratio of 0.60 and the average compressive strength of the concrete was 28 MPa used. One concrete cover depth was used, and the reinforcement bars were placed at the centres of the concrete samples. Another novel equation for bond strength prediction was developed by Chung et al. [4]. Here, pullout tests were conducted on concrete prisms prepared from a concrete mixture with a w/c ratio of 0.58 having a 28 day average concrete compressive strength of 28.3 MPa. One concrete cover depth was considered, and the reinforcement bars were embedded in the centres of the concrete prisms. The corrosion percentage was varied from 0% to 10%. In contrast to previous studies, Chung et al. [4] corroded the reinforcement bars before and after casting the concrete.

Although considerable research has been conducted to predict concrete bond strengths, contradictions are found in the literature. In particular, the degradation of bond strength due to corrosion and in concrete mixtures of different strength levels, taking into account the effect of differences in the concrete cover depths used, requires further investigation. Moreover, the available models (e.g., [2–5]) do not provide for the prediction of the ultimate bond strength as a function of a given concrete cover, crack width and concrete strength. The present study further extends these developments to evaluate the influence of concrete covers of three different depths (i.e., $c = 15$ mm, 30 mm and 45 mm) and two concrete strength levels (i.e., $f_c' = 23$ MPa and $f_c' = 51$ MPa) as upper and lower bound on the bond strength and bond-slip relationships for different corrosion levels. The corrosion percentage was varied from 0% for the control specimens to 18.75% for the corroded specimens. The new bond strength model developed in this work was then compared with previous models. In this study, single size bar was used and effect of cover-to-bar-diameter ratio (c/D ratio) on corrosion and bond strength were considered. The developed bond strength models in this study varied for concrete compressive strength between 23 MPa and 51 MPa for three different concrete cover depths; and do not directly represent the bond behaviour of reinforced concrete beams.

* Corresponding author: Tel.: +90 392630 1098; fax: +90 392630 2869.
E-mail addresses: hakan.yalciner@emu.edu.tr (H. Yalciner), ozgur.eren@emu.edu.tr (O. Eren), serhan.sensoy@emu.edu.tr (S. Sensoy).

0008-8846/$ – see front matter © 2012 Elsevier Ltd. All rights reserved.
doi:10.1016/j.cemconres.2012.01.003

Table 1
Concrete mixture proportions.

w/c	Cement (kg/m^3)	Water (kg/m^3)	Fine aggregate (kg/m^3)	Coarse aggregate (kg/m^3)			Average concrete compressive strength (MPa)
				10 mm	20 mm	40 mm	
0.40	563	225	716	160	240	477	51
0.75	300	225	965	162	243	485	23

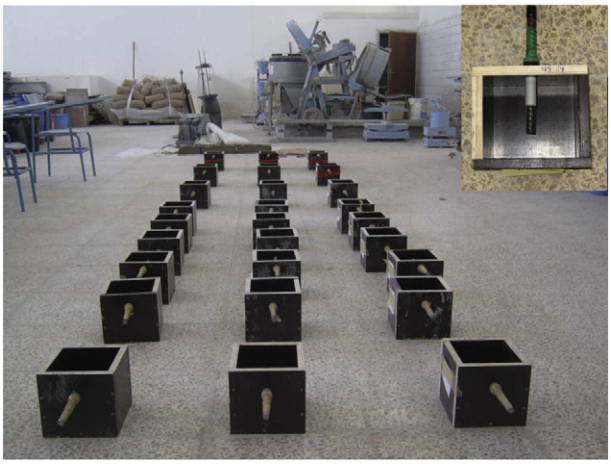

Fig. 1. Setup of the specimen moulds.

However, it is expected that the relationships obtained in this study will allow bond-slip modelling of reinforced concrete buildings to carry out seismic performance assessment and enhance previously developed models by using the same methodology (e.g., [2–5]).

2. Experimental program and test specimens

2.1. Experimental methods

A total of 90 specimens were tested in the current study. The experimental program consisted of two phases. In the first phase, different corrosion levels were investigated by considering the permeability of the concrete matrix and concrete covers. In this phase, the test specimens were divided into two main groups based on the type of concrete mixture used, with w/c ratios of 0.40 or 0.75. Each main group was subdivided into three smaller groups corresponding to the three different concrete covers: $c = 15$ mm, $c = 30$ mm and $c = 45$ mm. The samples in each subgroup were then subjected to corrosion for different time periods using an accelerated corrosion method. The contact resistivity was recorded for each specimen at one minute intervals to monitor the corrosion level. The crack width (W_{cr}) of the specimens was visually observed and measured with an EL35-2505 crack detection microscope. In the second phase, pullout tests were applied for each specimen to predict the ultimate bond strength and bond-slip relationships for different corrosion levels and considering the effects of different concrete covers and concrete strength levels.

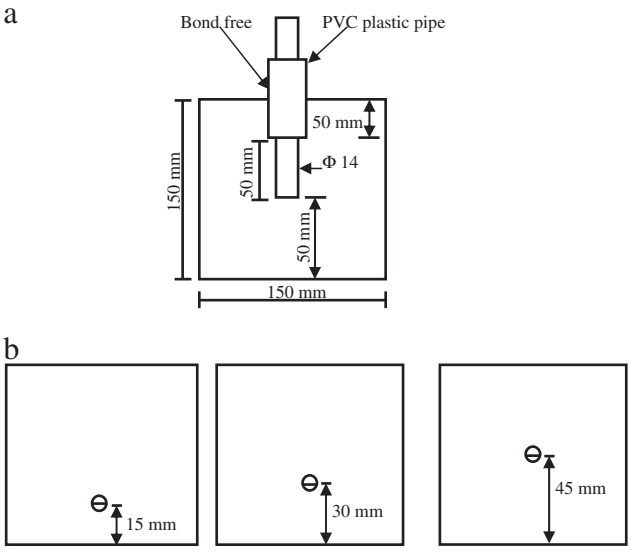

Fig. 2. Shapes of test specimens: (a) cross-section of mould; (b) top view for different bar locations.

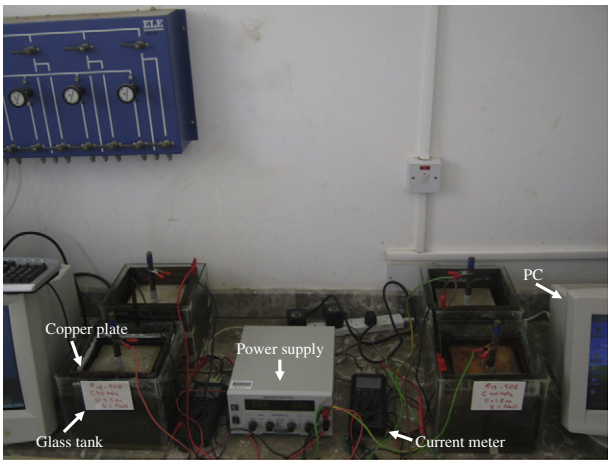

Fig. 3. Setup for the accelerated corrosion process.

2.2. Material properties

Deformed steel bars 14 mm in diameter and 250 mm long were used for all specimens. Tensile tests were performed on six randomly selected reinforcement bars, and the mechanical properties of the reinforcement bars were determined as follows: the yield strength (f_{sy}) was equal to 458 MPa, the rupture strength (f_{su}) was equal to 606 MPa, the yield strain (ε_{sy}) was equal to 0.00187, and the strain at the onset of strain hardening (ε_{sh}) was equal to 0.0299. Slag cement

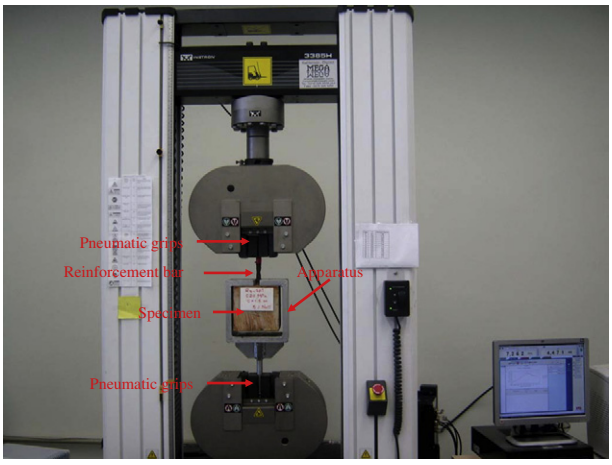

Fig. 4. Setup of the pullout testing system.

Table 2
Gravimetric test results of concrete mixtures with a water/cement ratio of 0.75.

Specimen	*c* (mm)	Faraday's mass loss (g)	Actual mass loss (g)	Corrosion level *CL* (%)	Applied corrosion time (h)	Maximum bond strength τ_{bu} (MPa)
R_1SP_1	15	Non-corroded	Non-corroded	–	–	9.1
R_1SP_2	15	Non-corroded	Non-corroded	–	–	9.4
R_1SP_3	15	Non-corroded	Non-corroded	–	–	9.2
R_2SP_1	30	Non-corroded	Non-corroded	–	–	14.0
R_2SP_2	30	Non-corroded	Non-corroded	–	–	12.3
R_2SP_3	30	Non-corroded	Non-corroded	–	–	13.5
R_3SP_1	45	Non-corroded	Non–corroded	–	–	12.1
R_3SP_2	45	Non-corroded	Non-corroded	–	–	17.3
R_3SP_3	45	Non-corroded	Non-corroded	–	–	15.0
R_4SP_1	15	38.28	26.00	8.90	97.00	3.7
R_4SP_2	15	10.45	12.00	4.10	72.00	13.0
R_4SP_3	15	9.67	7.20	2.47	108.05	11.2
R_4SP_4	15	9.52	7.97	2.72	95.00	11.7
R_4SP_5	15	13.92	12.66	4.32	72.00	12.2
R_4SP_6	15	14.27	12.69	4.33	72.00	12.2
R_4SP_7	15	13.46	11.98	4.09	72.00	13.0
R_4SP_8	15	21.58	19.07	6.51	85.00	3.2
R_4SP_9	15	67.54	42.54	14.52	120.00	2.1
R_5SP_1	30	3.98	4.00	1.37	97.00	18.0
R_5SP_2	30	10.08	10.00	3.45	169.00	9.6
R_5SP_3	30	19.21	16.00	5.56	202.00	3.3
R_5SP_4	30	4.38	4.10	1.40	97.00	17.9
R_5SP_5	30	5.40	4.95	1.69	97.00	16.9
R_5SP_6	30	5.07	4.69	1.60	97.00	17.0
R_5SP_7	30	11.26	10.46	3.57	169.00	8.9
R_5SP_8	30	16.90	15.70	5.36	202.00	3.7
R_5SP_9	30	68.58	48.78	16.65	216.00	2.1
R_6SP_1	45	3.20	2.00	0.69	97.00	19.1
R_6SP_2	45	6.11	5.00	1.69	210.53	13.4
R_6SP_3	45	10.74	7.60	2.66	330.48	12.4
R_6SP_4	45	2.34	1.99	0.68	216.00	17.9
R_6SP_5	45	2.26	1.93	0.66	216.00	18.9
R_6SP_6	45	2.82	2.47	0.84	266.00	18.3
R_6SP_7	45	2.92	2.58	0.88	266.00	18.2
R_6SP_8	45	5.06	4.68	1.60	270.00	13.7
R_6SP_9	45	11.47	11.15	3.81	200.00	1.3
R_7SP_1	15	301.40	57.00	18.75	289.15	4.3
R_7SP_2	15	49.39	26.60	8.90	216.00	3.0
R_7SP_3	15	84.69	42.80	14.66	120.00	2.0
R_8SP_1	30	30.51	20.40	6.87	288.98	6.5
R_8SP_2	30	74.81	52.00	17.33	216.00	1.8
R_8SP_3	30	25.02	27.00	6.40	190.27	5.5
R_9SP_1	45	24.92	19.00	6.27	289.18	3.2
R_9SP_2	45	2.36	2.00	0.68	216.00	18.0
R_9SP_3	45	10.68	11.40	3.81	200.50	1.3

Table 3
Gravimetric test results of concrete mixtures with a water/cement ratio of 0.40.

Specimen	*c* (mm)	Faraday's mass loss (g)	Actual mass loss (g)	Corrosion level *CL* (%)	Applied corrosion time (h)	Maximum bond strength τ_{bu} (MPa)
$R_{10}SP_1$	15	Non-corroded	Non-corroded	–	–	19.6
$R_{10}SP_2$	15	Non-corroded	Non-corroded	–	–	14.3
$R_{10}SP_3$	15	Non-corroded	Non-corroded	–	–	20.0
$R_{11}SP_1$	30	Non-corroded	Non-corroded	–	–	20.9
$R_{11}SP_2$	30	Non-corroded	Non-corroded	–	–	21.7
$R_{11}SP_3$	30	Non-corroded	Non-corroded	–	–	21.0
$R_{12}SP_1$	45	Non-corroded	Non-corroded	–	–	21.2
$R_{12}SP_2$	45	Non-corroded	Non-corroded	–	–	27.4
$R_{12}SP_3$	45	Non-corroded	Non-corroded	–	–	27.8
$R_{13}SP_1$	15	3.43	4.00	1.33	97.00	18.5
$R_{13}SP_2$	15	41.59	22.00	7.48	144.83	3.5
$R_{13}SP_3$	15	19.61	13.00	4.47	90.92	6.3
$R_{13}SP_4$	15	4.25	2.25	0.77	72.00	22.3
$R_{13}SP_5$	15	4.14	2.34	0.80	72.00	22.4
$R_{13}SP_6$	15	4.48	2.65	0.90	80.00	21.7
$R_{13}SP_7$	15	4.06	2.74	0.94	80.00	21.5
$R_{13}SP_8$	15	26.18	22.16	7.56	144.83	3.5
$R_{13}SP_9$	15	10.48	9.66	3.30	94.00	7.5
$R_{14}SP_1$	30	1.38	0.00	0.00	97.00	20.4
$R_{14}SP_2$	30	17.45	15.00	5.14	295.78	6.2
$R_{14}SP_3$	30	22.44	16.00	5.46	256.23	2.4
$R_{14}SP_4$	30	3.88	1.89	0.65	192.00	23.8
$R_{14}SP_5$	30	3.79	1.99	0.68	192.00	3.9
$R_{14}SP_6$	30	4.03	2.25	0.77	210.00	23.5
$R_{14}SP_7$	30	4.02	2.26	0.77	210.00	23.4
$R_{14}SP_8$	30	6.08	4.98	1.70	240.00	14.0
$R_{14}SP_9$	30	21.04	13.04	4.45	255.00	4.2
$R_{15}SP_1$	45	1.64	0.00	0.00	97.00	28.3
$R_{15}SP_2$	45	10.44	8.00	2.69	528.00	7.6
$R_{15}SP_3$	45	Not recorded	1.00	0.34	576.00	26.2
$R_{15}SP_4$	45	1.70	0.90	0.31	576.00	31.6
$R_{15}SP_5$	45	2.96	1.16	0.40	576.00	31.0
$R_{15}SP_6$	45	2.61	1.21	0.41	576.00	30.8
$R_{15}SP_7$	45	16.48	13.87	4.73	816.00	3.0
$R_{15}SP_8$	45	15.38	12.83	4.38	816.00	3.4
$R_{15}SP_9$	45	14.62	12.20	4.17	816.00	3.9
$R_{16}SP_1$	15	43.80	26.40	8.95	288.57	3.0
$R_{16}SP_2$	15	24.21	20.00	6.90	216.00	8.0
$R_{16}SP_3$	15	12.93	10.00	3.41	4.00	6.8
$R_{17}SP_1$	30	37.46	29.00	9.90	289.03	5.9
$R_{17}SP_2$	30	23.34	14.00	4.86	216.00	1.7
$R_{17}SP_3$	30	5.29	5.00	1.72	242.00	13.8
$R_{18}SP_1$	45	3.38	1.00	0.34	289.03	26.9
$R_{18}SP_2$	45	Not recorded	1.00	0.34	576.00	31.7
$R_{18}SP_3$	45	14.13	9.00	3.08	816.00	6.1

42.5 was used with crushed limestone aggregate. Table 1 shows the mixture proportions of concrete for the two different concrete strengths. In Table 1, the water contents given are the net water contents after considering moisture adjustments. No air-entraining or water-reducing admixtures were used. The prepared concrete mixes were cast in 150 mm cubes made of waterproof plywood. Fig. 1 shows the setup for the 27 concrete specimens with a *w*/*c* ratio of 0.40 before casting the concrete.

2.3. Mixing, casting and curing

Before mixing the concrete, the reinforcement bars were carefully cleaned. The mass of the reinforcement bars in each specimen was

Fig. 5. Corroded reinforcement bars after cleaning.

recorded, and the bars were aligned and fastened to the moulds. A mould-releasing compound was applied to the inside surfaces of the specimen moulds. Compaction was performed with a table vibrator. After pouring and compacting the concrete, the specimen surface was smoothed with a steel trowel. The concrete specimens were kept in a curing room maintained at 22 °C (±2 °C) and 90% relative humidity for 24 h. Demoulding and transportation of the specimens were conducted with great care to avoid any disturbance of the reinforcement bars. After demoulding, the specimens were cured in a water tank at 22 °C (±2 °C) for 28 days.

2.4. Accelerated corrosion method

An electrochemical method was used to accelerate the corrosion of the reinforcement bars. The specimens were fully immersed in an aqueous solution of 3.5% sodium chloride by weight for four days before being subjected to the accelerated corrosion procedure. Before and during this procedure, the temperature of the water over each concrete specimen was held constant at 22 °C (±2 °C). The shapes of specimens representing the three different concrete covers are shown in Fig. 2.

As shown in Fig. 2(a), deformed reinforcement bars 14 mm in diameter were placed in the cubes with different concrete covers. The embedded length was set at 50 mm to ensure bond failure. To prevent contact between the concrete and the reinforcement bars while maintaining the required concrete cover on the surface of the concrete specimen, 50 mm lengths of the reinforcement bars were placed inside polyvinyl chloride (PVC) pipes. The specimens were then fully immersed in a glass tank filled with water. An adjustable direct current supply providing 60 V constant potential at 0 to 5 A was used for the accelerated corrosion process. The direct current was applied to the main reinforcement bar embedded in the concrete, using the reinforcement bar as the anode and a copper plate as the cathode. The current was passed from the reinforcement bars to the copper plate placed inside of 5% salt solution (NaCl). The setup for the accelerated corrosion process is shown in Fig. 3.

The designed (theoretical) mass loss of the reinforcement bars due to corrosion was calculated according to Faraday's law using Eq. (1):

$$\text{mass loss} = \frac{t(s) \times I(A) \times 55.847(\text{g/mol for iron})}{2 \times 96,487(\text{coulomb})} \quad (1)$$

where t is the time, I is the current, 55.847 (g/mol) is the molar mass for iron and 96,487 (coulomb) is the Faraday's constant. The actual corrosion level or percentage mass loss of each specimen was calculated by Eq. (2):

$$C_L = \frac{G_0 - G_1}{G_0} \times 100\% \quad (2)$$

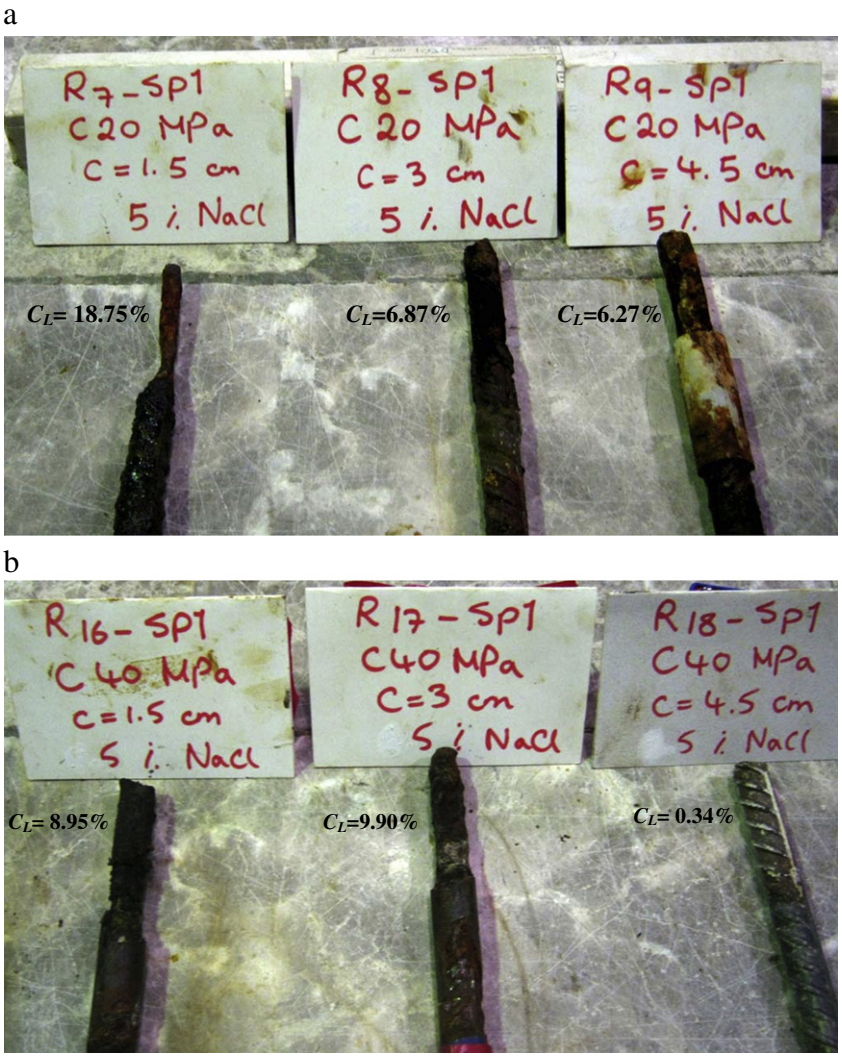

Fig. 6. Effect of concrete cover depth on corrosion level: (a) $w/c = 0.75$; (b) $w/c = 0.40$.

where G_0 is the initial weight of the reinforcement bars before corrosion and G_1 is the weight of the reinforcement bars after the removal of the corrosion products.

3. Pullout tests

Pullout tests were performed for both corroded and uncorroded specimens based on ASTM C234-91a [6]. The bond tests were performed with an Instron model 3385H universal testing machine with a capacity of 250 kN. The applied loads were controlled via computer, using displacement control at a rate of 10 mm/min. The setup of the pullout testing system is shown in Fig. 4.

As shown in Fig. 4, this apparatus was especially designed and adapted to avoid any changes in bond strength during the pullout test. The results of the displacement and stress values of the designed apparatus at any point was negligible under an applied 25 kN load. None of the reinforcement bars reached the yield point during the pullout tests, and the maximum pullout forces were recorded to calculate the ultimate bond strength (τ_{bu}) according to Eq. (3):

$$\tau_{bu} = \frac{P_{\max}}{\pi DL}(MPa) \tag{3}$$

where $P_{\max}$ is the ultimate pullout load and D and L are the diameter and bond length of the reinforcement bars, respectively.

4. Experimental results

The specimens were designated R_1SP_1 to R_9SP_3 for the concrete specimens having w/c ratios of 0.75 (see Table 2) and $R_{10}SP_1$ to $R_{18}SP_3$ for the concrete specimens having a w/c ratio of 0.40 (see Table 3). The specimen was named such as R_1SP_1, where R stands for different w/c ratio and cover depth, and SP stands for specimen number. The test results were analysed for the following parameters:

- Applied corrosion levels and the effects of concrete covers and strengths on corrosion levels
- A comparison between theoretical and actual corrosion mass losses
- Concrete resistivity
- The effects of corrosion levels, concrete covers, crack width and concrete strengths on bond strength
- Bond-slip relationships at different corrosion levels

4.1. Applied corrosion levels and the effects of concrete covers and strengths on corrosion levels

To calculate the mass losses of the reinforcement bars, chemical cleaning was performed using hydrochloric acid to remove the corrosion products from the surface of the reinforcement bars, according to ASTM G1-03 [7]. Fig. 5 shows selected corroded reinforcement bars after the pullout tests.

Tables 2 and 3 show the gravimetric test results and comparisons between the theoretical and actual mass losses of specimens with w/c ratios of 0.75 and 0.40, respectively.

Fig. 6(a–b) shows the effect of concrete cover depth on the corrosion level for samples with the same w/c ratios under the same applied corrosion time ($t = 289$ h). As shown here and in Tables 2 and 3, the effect of concrete cover depth on the corrosion level was significant; increasing concrete cover depth decreased the corrosion level.

Even though plastic pipes were used to prevent contact between the concrete and the reinforcement bars on the surface of the concrete specimens, local corrosion occurred for some specimens at the outside of the concrete. As shown in Fig. 6(a–b), corrosion of the reinforcement that occurred outside of the concrete led to higher mass loss for specimen $R_{17}SP_1$ than R_8SP_1, even though more mass loss would be expected for R_8SP_1 due to its higher w/c ratio (and presumed higher permeability). The differences in the corrosion levels obtained at a fixed corrosion time showed that more energy was needed to initiate corrosion in the concrete mixture with a w/c ratio of 0.40 than that with a w/c ratio of 0.75. Fig. 7(a–c) illustrates the effects of both concrete covers and w/c ratios on the corrosion levels for different applied corrosion times for selected specimens. Here, for the same applied corrosion time, the corrosion level decreased with increasing concrete cover depth. The reduced permeability of the concrete with the 0.40 w/c ratio likely reduced corrosion of the reinforcement bars, because increasing the w/c ratio increases capillary porosity [8]. As shown in Fig. 7(a–b), due to the premature cracking of $R_{16}SP_3$ and R_8SP_2 compared with $R_{13}SP_1$ and R_8SP_1, respectively, more corrosion was observed at an earlier stage due to the increased permeability of the concrete in the former. The recorded concrete resistivity values were used to estimate the time required for the growth of fine cracks (t_{cr}). For instance, the resistivity of R_8SP_2 began to decrease at 70 h, whereas it decreased at 105 h for R_8SP_1.

It should be noted that concrete resistivity and premature cracking had no influence on the bond strength. Therefore, the corrosion

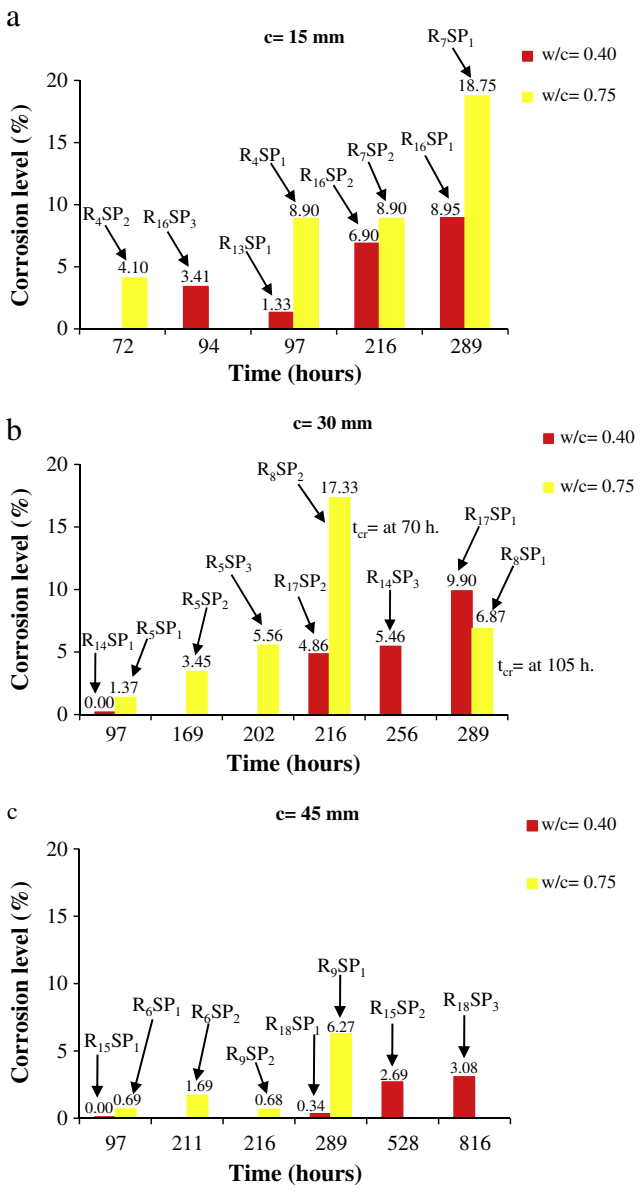

Fig. 7. Effect of concrete cover depth and w/c ratio on corrosion level: (a) $c = 15$ mm; (b) $c = 30$ mm; (c) $c = 45$ mm.

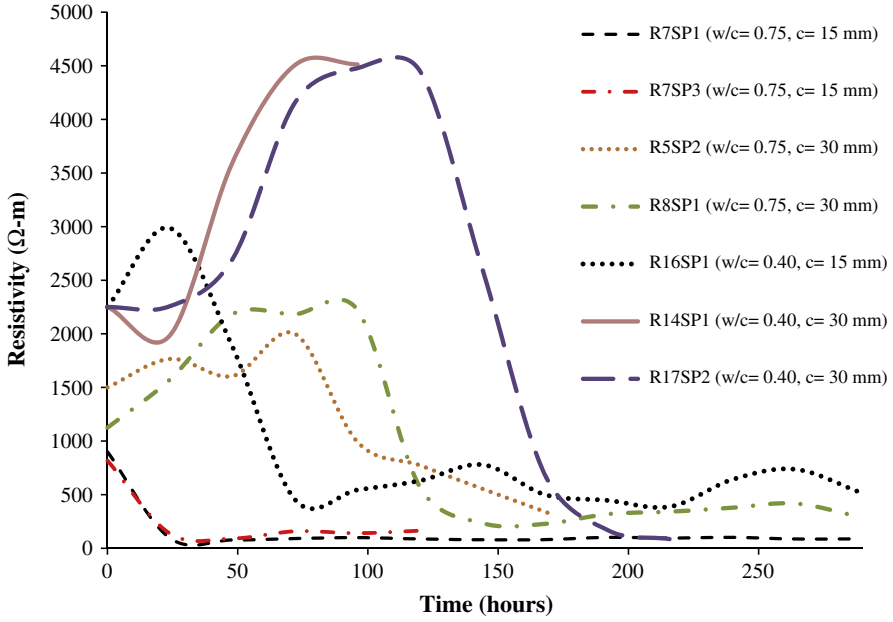

Fig. 8. Relationship between resistivity of concrete and time.

levels determined from the actual mass losses in the reinforcement bars and the recorded concrete crack widths were used to develop the proposed strength model.

4.2. Comparison between theoretical and actual corrosion mass losses

Comparing the results given in Tables 2 and 3, there were differences between the measured and theoretically estimated corrosion mass losses based on Faraday's law. Such differences have been reported previously in the literature (e.g., [1,9]). However, in this study, different concrete classes and concrete cover depths were evaluated; thus, upper and lower bounds for the correlation between the actual and theoretically estimated mass losses were obtained. By considering the typical environmental conditions used in our experiments, Eq. (4) can be used to correlate the actual and theoretically estimated mass losses in future studies.

$$\text{Actual mass loss} = 0.703 \times \text{theoretical mass loss} - 0.15(\text{gr})R^2 = 0.94 \quad (4)$$

4.3. Concrete resistivity

Although the concrete resistivity was not our main interest in this study, it was used to monitor the corrosion level. Under the same environmental conditions, the relationships between concrete resistivity and corrosion time for both the low and high strength concrete levels were determined, as shown in Fig. 8.

The resistivity results obtained by calculating the average current over 24 h from the current recorded at one-minute intervals are presented in Fig. 8. The results clearly show that reducing the *w/c* ratio of the concrete was more effective than increasing the concrete cover depth for improving the protection against chloride attack provided by the concrete. Fig. 8 shows the resistivities of specimens R_5SP_2 and R_8SP_1 ($w/c = 0.75$ and $c = 30$ mm); although they had a 30 mm concrete cover, the measured resistivity for these concretes suggests lower protection against chloride attack than that of the concrete specimens with the lower *w/c* ratio and a 15 mm concrete cover depth (e.g., $R_{16}SP_1$). Thus, a 50% reduction in concrete cover depth with the lower *w/c* ratio provided 34% more resistivity than the higher *w/c* ratio. It was observed that the resistivity increased quickly during the initial period of the corrosion process; this continued for a long time, and then the resistivity dropped quickly beginning with the initiation of visible surface cracks. However, in the concrete specimens R_7SP_1 and R_7SP_3, the resistivity started to drop at the beginning of corrosion process, likely due to the closer contact surface of the reinforcement bars. Although the concrete specimens were cured under the same conditions, due to the complex concrete matrix, including many unknown variables, nonuniform corrosion behaviour was observed during the accelerated corrosion procedure. In this study, only two concrete specimens (i.e., R_7SP_2, R_9SP_1) displayed this nonuniform behaviour.

4.4. Developed bond strength model

The ultimate bond strengths of corroded and uncorroded specimens were calculated using the initial cross-sectional dimensions of the reinforcement bars. Fig. 9 shows the relationship between concrete compressive strength and the maximum bond strength for different concrete covers in the case of uncorroded specimens.

The values given in Fig. 9 are the average bond strengths of 18 concrete specimens for each concrete strength level. As shown here, the bond strength depends on both the concrete compressive strength and the concrete cover depth. The results showed that up to a *c/D* ratio of 3.2, the bond strength increased with increasing

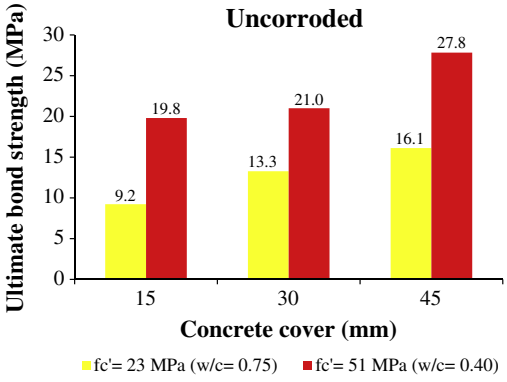

Fig. 9. Ultimate bond strengths of uncorroded specimens.

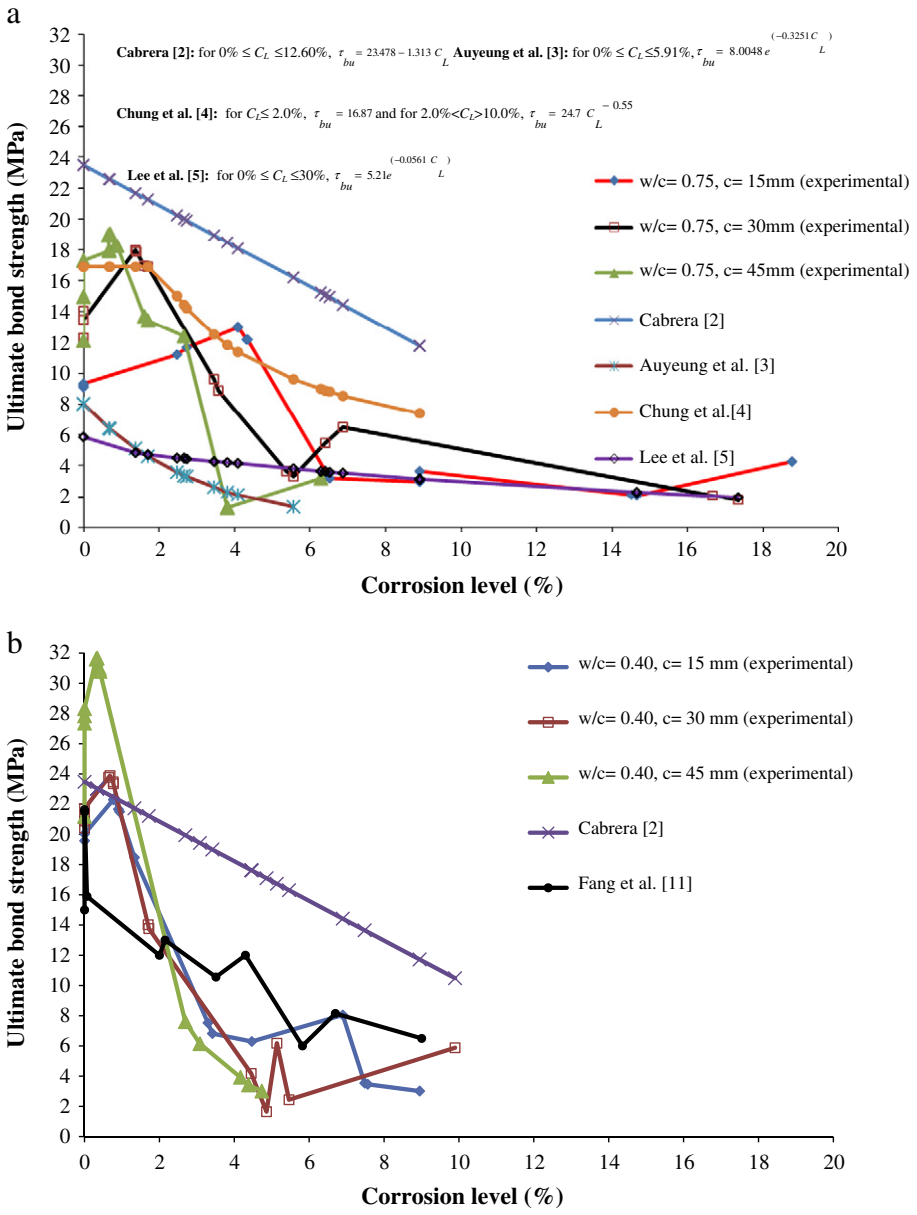

Fig. 10. Bond strengths of corroded specimens: (a) $w/c = 0.75$; (b) $w/c = 0.40$.

concrete compressive strength, and no significant increase was recorded for the c/D ratios above 3.2. As shown in Fig. 9, the effect of concrete cover depth on bond strength was more significant in the concrete specimens of lower concrete strength level. For example, when the concrete cover depth was increased from 15 mm to 30 mm, the bond strength of the concrete with a w/c ratio of 0.75 was increased by 43.7%, whereas it increased 6% for the concrete specimens having a w/c ratio of 0.40. With further increases in concrete cover depth, differences in bond strength increases between the two concrete strengths were moderate. For example, when the concrete

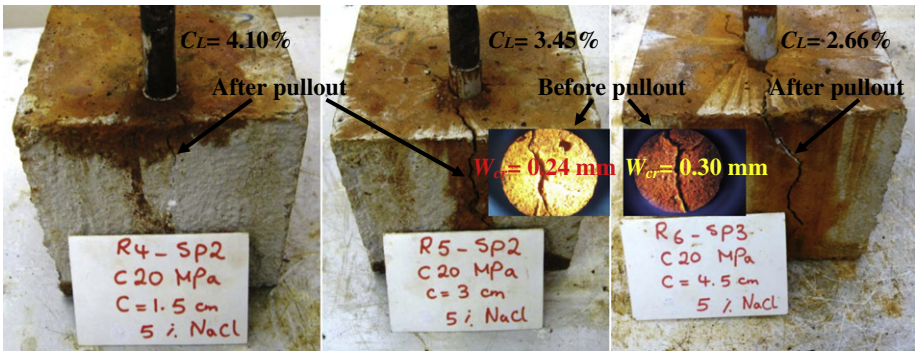

Fig. 11. Effect of cover-to-diameter ratio on concrete cracking (see video 1).Effect of cover-to-diameter ratio on concrete cracking (see video 1).

cover depth was increased from 15 mm to 45 mm, the bond strengths of concrete specimens with w/c ratios of 0.40 and 0.75 increased by 41% and 52%, respectively. As expected, for concrete covers of the same depth, bond strength increased as the w/c ratio was reduced. On reducing the w/c ratio from 0.75 to 0.40, bond strengths increased by 58% and 73% with concrete covers 30 mm and 45 mm thick, respectively. In the case of the uncorroded specimens, increasing the concrete compressive strength with a given concrete cover depth yielded a higher bond strength than increasing the concrete cover depth for a given concrete strength. The following equation was developed to predict the ultimate bond strength of uncorroded specimens using linear regression analysis, where the coefficient of correlation (R^2) was 0.96.

$$\tau_{bu} = -2.7143 + 0.3621 f_c{}' + 2.3296\left(\frac{c}{D}\right)(\text{MPa}) \quad (5)$$

In contrast to previous models, the model developed in Eq. (5) provides a way to predict the ultimate bond strength not only as a function of concrete strength but also as a function of the c/D ratio.

Fig. 10a and b show the bond strengths of corroded reinforcement bars with ratios of $w/c = 0.75$ and $w/c = 0.40$, respectively.

In the studies by Auyeung et al. [3] and Chung et al. [4], the bond strength relationships for corroded reinforcement bars are defined by two segments with a limiting corrosion level. However, there is disagreement on this corrosion level limit. Auyeung et al. [3] reported that bond strength decreases rapidly when the corrosion mass loss exceeds 1%, whereas it was reported by Chung et al. [4] that increases in bond strength are negligible up to a corrosion level of 2%. The results of the present study showed that bond strengths in corroded specimens depend on the c/D ratio, the concrete compressive strength and the crack width. An interesting result was obtained for the lower-strength concrete at the lowest c/D ratio ($w/c = 0.75$ and $c = 15$ mm). As shown in Fig. 10(a), up to a corrosion level of 4%, bond strength increased and then decreased for a given corrosion level. However, increases in bond strength occurred at lower levels of corrosion with higher c/D ratios. For the low levels of corrosion, the average bond strength likely increased due to the increased roughness of the steel bar caused by the confined corrosion products [9]. Our results showed that this phenomenon was more obvious when greater confinement of the bar in the concrete is encountered during pullout testing. For example, in Fig. 10(a), the bond strength at the lowest c/D ratio increased by approximately 41% at a corrosion level of 4%. For a higher c/D ratio ($c/D = 2.143$ or $c = 30$ mm), bond strength was increased by 51% at the lower corrosion level of 1.4% and then decreased nonlinearly beyond 1.4%. This can be explained by the frictional properties of the interface between the reinforcement bars and the concrete and by the crack width. The lugs of the reinforcement bars at the lowest c/D ratio were highly corroded, which decreased the transfer of stress from the reinforcement bars to the surrounding concrete. With respect to these results, it should be noted that the cracking of concrete increased with concrete depth. Fig. 11 shows the effect of various c/D ratios on concrete cracking after the pullout tests.

As shown in Fig. 11, crack width increased with increasing c/D ratio at the lower corrosion levels when compared with lower c/D ratios at higher corrosion levels. For example, in Fig. 11, even though the corrosion level of R_4SP_2 was 54% more than that of R_6SP_3, the observed crack width was wider for R_6SP_3 after the pullout test. As shown in Fig. 10(a), for the same w/c ratio, an increase in the c/D ratio yielded a different behaviour than at the lower c/D ratio. The likely reason for this is that the cracks observed in the specimens with the higher c/D ratio caused a reduction in bond strengths at lower corrosion levels. After the accelerated corrosion process, the maximum recorded crack widths on the surfaces of R_5SP_2 and R_6SP_3 were 0.24 mm and 0.30 mm, respectively, whereas no cracks were observed on R_4SP_2 (Fig. 11).

Another important result of this study was the observation that with increasing concrete compressive strength, the degradation of bond strength at higher concrete strengths was more than that with lower-strength concrete (see Fig. 10(b)). The specimens with higher-strength concrete became more brittle than in the uncorroded condition where sudden loss of bond strength occurred. Chang [10] reported that bond degradation is more significant for concrete with a higher w/c ratio. However, the data reported by Lee et al. [5] and in the present study disagrees with that given by Chang [10]. Fig. 12 shows the reductions in bond strengths for two concrete strength levels at almost the same corrosion levels.

Based on the results shown in Fig. 12 and given the bond-slip relationships in the next section, it is clear that the effect of corrosion is more dramatic in concrete with a higher strength level. The measured maximum crack widths on the surface of the concrete samples clearly support this interpretation. At the same corrosion levels, the maximum crack width of the high-strength concrete was greater than that in the low-strength concrete during the accelerated corrosion process. As shown in Fig. 12, the crack width of $R_{15}SP_2$ was 0.80 mm, whereas the crack width of R_6SP_3 was 0.30 mm (see Fig. 11) at almost the same corrosion level.

In Fig. 10(a–b), the experimental results of this study are compared with the previously developed models found in the literature. As shown in Fig. 10(b), Fang et al. [11] did not provide an equation to predict the ultimate bond strength. Therefore, the available

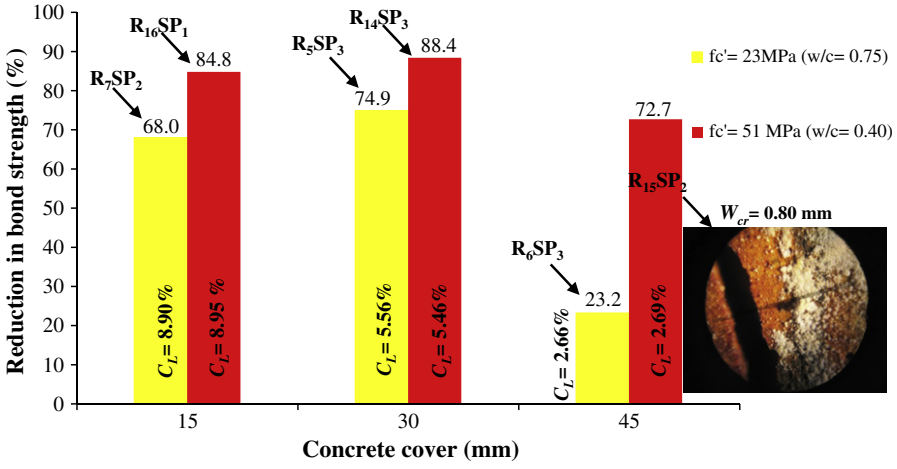

Fig. 12. Reduction in bond strength.

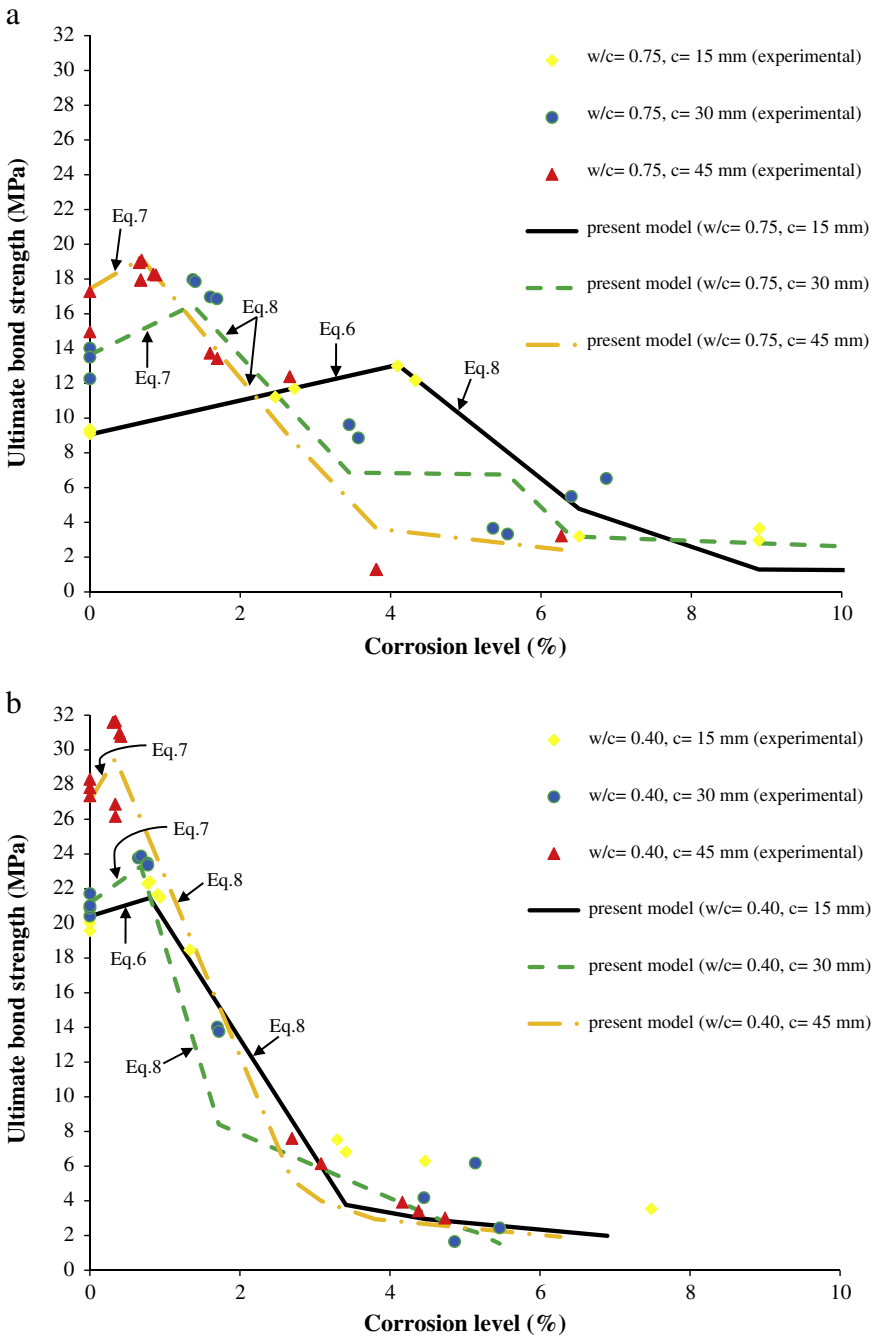

Fig. 13. Validation of proposed models: (a) $w/c = 0.75$; (b) $w/c = 0.40$.

experimental data from the pullout tests done by Fang et al. [11] were directly plotted in Fig. 10(b); the concrete strength in this study was 52.1 MPa. This comparison shows that the previous empirical bond strength equations underestimate or overestimate bond strengths for different conditions. Among them, the latest study by Chung et al. [4] gave better results. It should be noted that in the study of Chung et al. [4] the reinforcement bars were corroded before and after casting in concrete, and a single concrete strength and a single concrete cover depth were evaluated.

As shown in Fig. 10(a), the previous empirical models developed (e.g., [2,3,5]) predict that the bond strength should decrease with increasing corrosion level, but these models do not represent the actual corrosion behaviour, especially when different c/D ratios and concrete strengths are taken into account. As a result of combining different c/D ratios and concrete strengths to predict the bond strength, the following equations were obtained using linear and nonlinear regression analysis. To accurately predict the ultimate bond strength, the developed models were separated into two parts. Considering the scatter in the experimental data, two equations were derived for the ascending branch (see Eqs. (6) and (7)) based on the c/D ratios and the given limits of the corrosion levels.

$$\text{if} \, c/D < 2 \text{ and } {}^{0 \le C_L \le 4 \text{for} f_c' = 23 MPa}_{0 \le C_L \le 0.8 \text{for} f_c' = 51 MPa}$$
$$\tau_{bu} = 0.40551 f_c{}' - 0.25306 \left(\frac{c}{D}\right) + 0.97926 C_L (\text{MPa}) \left(R^2 = 0.98\right) \quad (6)$$

$$\text{if } c/D \geq 2 \text{ and } \begin{matrix} 0 \leq C_L \leq 1.4 \text{ for } f_c' = 23\text{MPa} \\ 0 \leq C_L \leq 0.68 \text{for } f_c' = 51\text{MPa} \end{matrix}$$
$$\tau_{bu} = e^{\left(0.01572 f_c' + 0.22957\left(\frac{c}{D}\right) + 0.13946 C_L + 1.75913\right)} (\text{MPa}) \left(R^2 = 0.94\right) \quad (7)$$

For the descending branch of the bond strength curve in Fig. 10(a–b), the relation is given by Eq. (8). If the corrosion levels are above the limits given by Eqs. (6) and (7), the proposed Eq. (8) can be used to calculate the bond strength for the descending branch. In other words, if $1 \leq c/D \leq 3.2$, then:

$$\tau_{bu} = e^{\left(0.01667 f_c' - 1.06499 W_{cr} + 0.20658 \frac{c}{D} - 0.12928 C_L + 1.80139\right)} (\text{MPa}) \left(R^2 = 0.96\right) \quad (8)$$

can be used conveniently.

The experimentally obtained results were compared with those obtained with the proposed analytical models, as shown in Fig. 13(a–b). As shown in Fig. 13(a–b), it is possible to predict the bond strength as a function of crack width and corrosion levels for different c/D ratios and concrete strengths in the light of developed bond strength models and their limitations. As shown in Fig. 10(a), whereas previous models show a decrease in bond strength with increasing corrosion level, the newly proposed model shows a more realistic behaviour reflecting the actual bond strength. Using the relations given by Eqs. (6)–(8), it is possible to monitor bond strength behaviour at both low and high corrosion levels with cracked or uncracked concrete conditions for different c/D ratios and concrete strengths.

4.5. Bond-slip relationships

The bond-slip relationships for selected uncorroded specimens are shown in Fig. 14. Here, the slippage of the reinforcement bars decreases with increasing c/D ratio and concrete strength. The results presented in Fig. 14 are in accord with the relationships obtained for bond strength. It can be seen in Fig. 14 that the peak of the curve of the high-strength concrete is relatively sharp, but the curve has a flat top for the low-strength concrete. The results show that at the same applied load, slip displacement was less for the higher-strength concrete than for the lower-strength concrete. Moreover, the c/D ratio has a significant effect on the slip displacement, which tends to decrease with an increasing c/D ratio. For example, in Fig. 14, the slip displacement at the maximum bond strength of R_1SP_1 was reduced by 35% due to the increased c/D ratio of R_3SP_2. For the same concrete cover depth ($c = 30$ mm), the recorded slip displacement at the maximum bond strength of R_2SP_2 was reduced by 20% with an increase in concrete compressive strength for $R_{11}SP_2$. Similarly, comparing the two concrete strength levels at a 45 mm cover depth, the slip displacement at maximum bond strength of R_3SP_2 was reduced by 19% from that of the higher-strength $R_{12}SP_2$. Thus, it can be said that percentage reduction in slip displacement with changing cover depths were almost the same among different strength levels for the uncorroded specimens.

The bond-slip relationships for corroded specimens are given in Fig. 15(a–b). These relationships are important in verifying our findings regarding the bond strength degradation of higher-strength concrete due to corrosion. As shown in Fig. 15(a), when the c/D ratio was less than two ($c = 15$ mm), more slip displacement occurred at lower corrosion levels for higher-strength concrete due to the opening of longitudinal cracks during the pullout tests. As mentioned earlier, the occurrence of cracks during accelerated corrosion played an important role in the case of the corroded specimens. In Fig. 15(a), the measured maximum crack width on the surface of $R_{16}SP_3$ was 0.6 mm, whereas no cracks were observed on R_4SP_3 and R_4SP_2. In Fig. 15(a), the slip displacement of R_1SP_2 at the maximum bond strength was reduced by 48% due to the increased corrosion level of R_4SP_2 (4%). However, at the maximum bond strength of the higher-strength concrete ($R_{16}SP_3$), the slip displacement increased by 34% at the lower corrosion level of 3.4%. In Fig. 15(a), it can be seen that when the corrosion level was relatively a large value (e.g., R_4SP_1 and $R_{16}SP_1$), the effect of corrosion on slip displacement was almost the same for the different concrete strength levels due to more localised and extensive cracking of the concrete surface during the pull-out test. As illustrated in Fig. 15(b), the bond-slip relationship

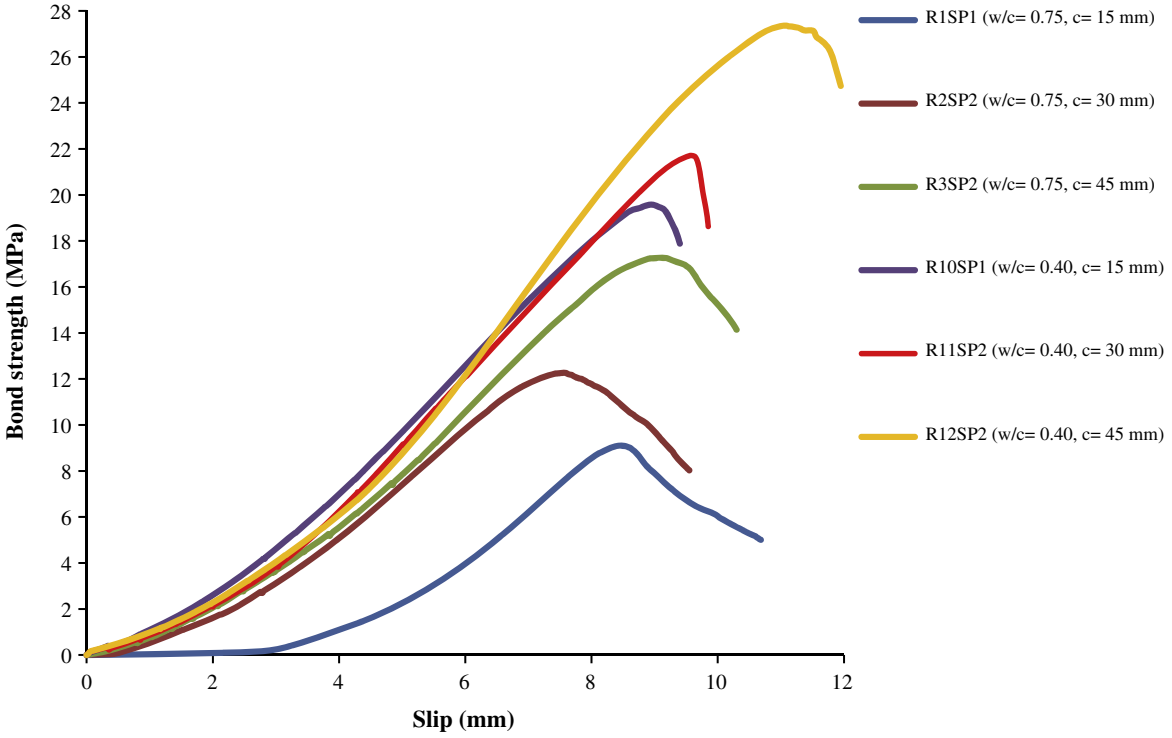

Fig. 14. Bond-slip relationships of uncorroded specimens.

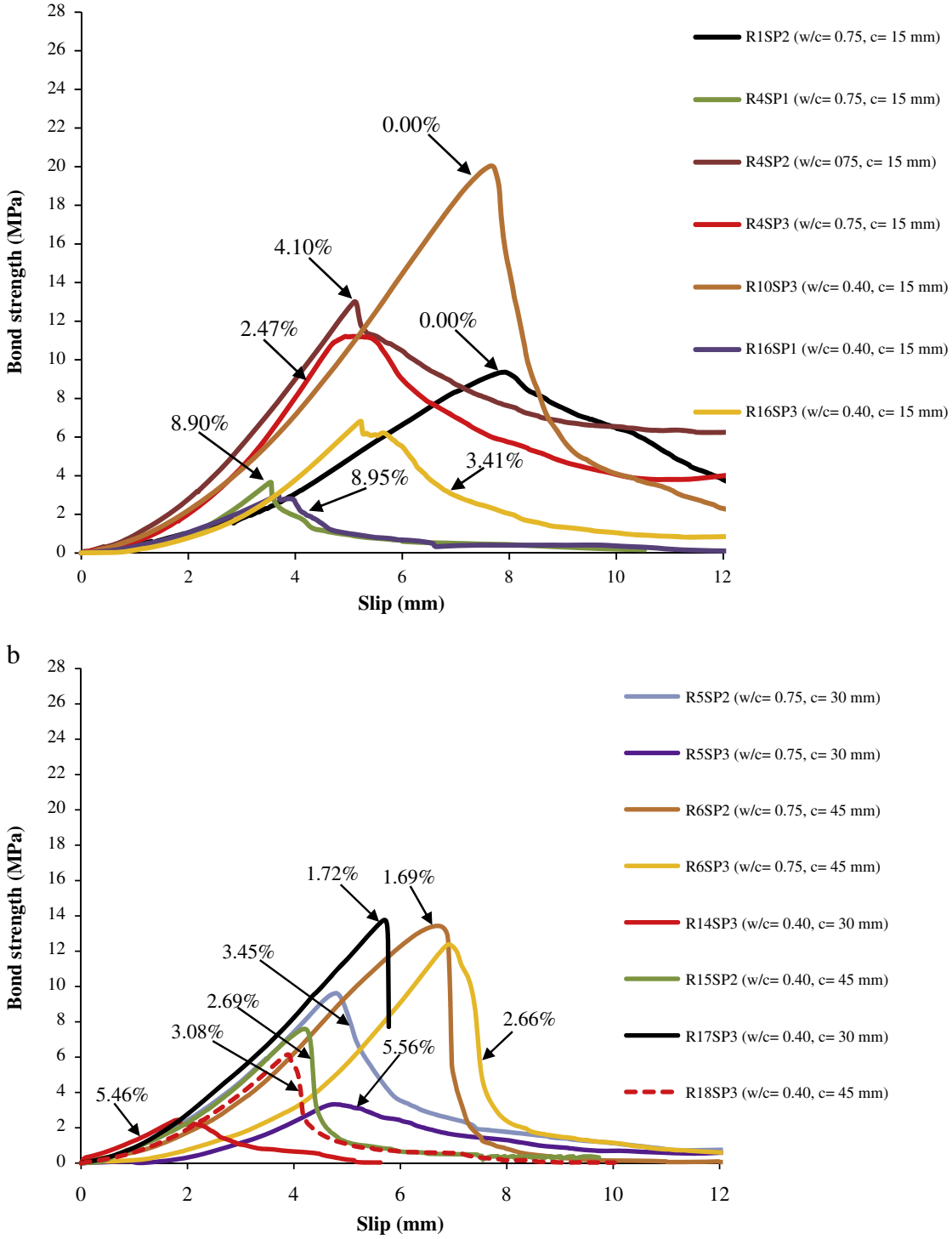

Fig. 15. Bond-slip relationships of corroded specimens: (a) $c = 15$ mm; (b) $c = 30$ mm and 45 mm.

showed different behaviours with increasing c/D ratio for the two different concrete strength levels. As shown in Fig. 15(b), the bond strength with the higher w/c ratio was greater than that with the lower w/c ratio at almost the same corrosion level (see R_6SP_3 and $R_{15}SP_2$). However, the results were different for slip displacement. When the slip displacements for the two concrete strength levels are compared for the same concrete cover depth ($c = 30$ mm), e.g., R_5SP_3 and $R_{14}SP_3$, it can be seen that less displacement occurred in the higher-strength concrete at an almost identical corrosion level. Similar results were also observed for several other specimens, such as R_6SP_3 and $R_{15}SP_2$, with a concrete cover of 45 mm. This can be explained by the increased resistance to the slippage of the reinforcement bars set in higher-strength concrete until the time it split. In Fig. 16(a–b), splitting of the concrete specimens along the corrosion cracks is shown. As shown in Fig. 16, at the almost same corrosion levels, wider cracks occurred for higher-strength concrete, which caused a loss of bond strength. Up to a given value of applied load, the higher-strength concrete provided less displacement, but for further increases in load it exhibited more brittle behaviour, with a sharp decrease occurring at the peak of the curve, as displayed by specimen $R_{17}SP_3$. A good relationship was obtained when the results were compared for different concrete cover depths. Fig. 15(b) shows that with a

a

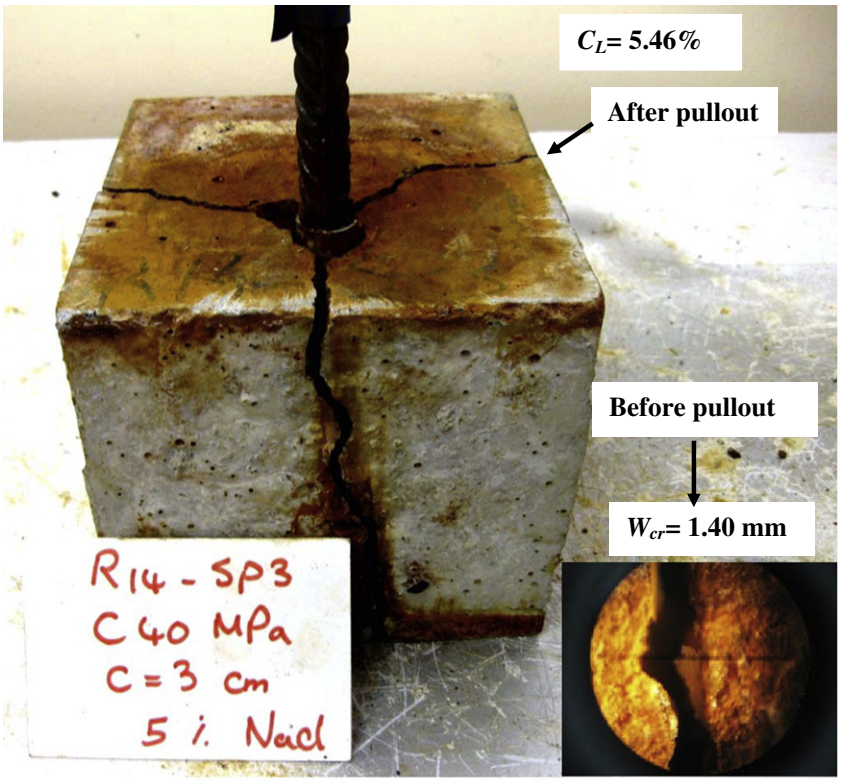
C_L= 5.46%
After pullout
Before pullout
W_{cr}= 1.40 mm
R14 - SP3
C40 MPa
C = 3 cm
5 i. NaCl

b

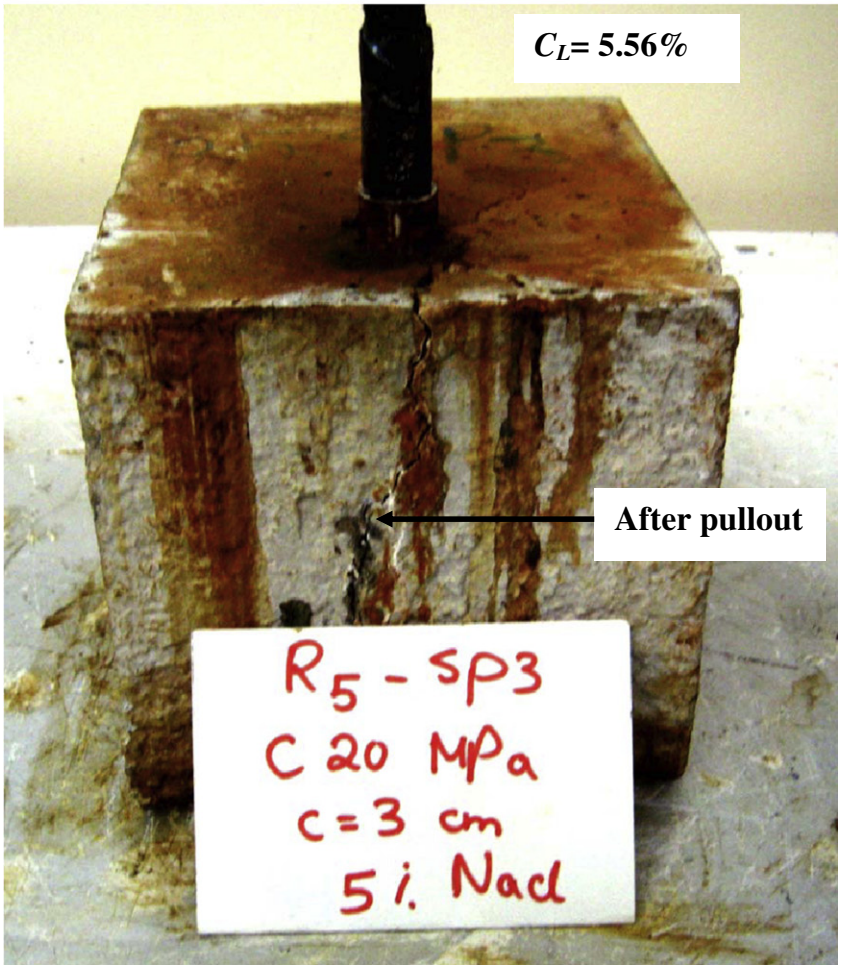
C_L= 5.56%
After pullout
R5 - SP3
C 20 MPa
C = 3 cm
5 i. NaCl

concrete cover depth of 30 mm and $w/c = 0.75$ (R_5SP_2), the value of slip displacement was almost the same at the maximum bond strength of $R_{15}SP_2$ ($c = 45$ mm and $w/c = 0.40$) at a higher corrosion level of 3.45%. The same behaviour was also observed with R_6SP_2 and $R_{17}SP_3$. In contrast with the previous samples (R_5SP_2, $R_{15}SP_2$), slip displacement was less for the higher-strength concrete ($R_{17}SP_3$) at the almost same corrosion level due to a lower cover depth.

5. Conclusions

A series of tests was performed to develop models for the prediction of the ultimate bond strengths of corroded and uncorroded reinforced concrete specimens. Based on the test results, the following conclusions were drawn:

1. Using the newly developed bond strength equations, based on the limitations specified before, it is possible to predict the bond strength as a function of corrosion levels, concrete strength levels, crack width and c/D ratios.
2. Previously developed bond strength equations yielded significantly underestimated or overestimated results; the bond strength decreases rapidly in these models.
3. In the case of the uncorroded specimens, bond strength increased with increasing concrete strength level and c/D ratio, where the c/D ratio of 3.2 and a w/c ratio of 0.40 yielded the highest ultimate bond strength in this study.
4. In the case of the uncorroded specimens, bond strength increased up to a c/D ratio of 3.2, and no significant enhancement observed above this ratio.
5. When the c/D ratio was increased in the uncorroded specimens, the percentage increase in ultimate bond strength of the lower-strength concrete was more than that of the higher-strength concrete. Indeed, this is a normal behaviour since the reinforcement bars used were deformed. The radial pressure from the lugs of the reinforcing bars causes high tensile stresses on concrete. The resistance of the specimen to these radial stresses depends on both the compressive strength and c/D ratio. Thus, as the c/D ratio increases for lower-strength level of concrete, resistance to these radial pressure will increase.
6. In the case of the uncorroded specimens, increasing the concrete compressive strength for a given concrete cover depth yielded higher bond strength than increasing the concrete cover for a given concrete strength.
7. At the same corrosion level, the measured maximum surface crack width of the higher-strength concrete was more than that of the lower-strength concrete. This was due to higher permeability of concrete specimens with higher w/c ratios of 0.75. Accelerated corrosion method showed that with a higher w/c ratio, the corrosion products were flowing throughout the concrete. Meanwhile, the colour of water in glass tank was changed to red. On the other hand, lower permeability of concrete ($w/c = 0.40$) maintained expansive corrosion products. These products increased the internal pressure which resulted in premature cracking of concrete due to volumetric expansion.
8. The splitting of the higher-strength concrete was more dramatic than that of the lower-strength concrete at the same corrosion level since initial cracks have been already observed during accelerated corrosion method as explained above.
9. An increase in crack width was observed with increasing c/D ratio at lower corrosion levels when compared with a lower c/D ratio at higher corrosion levels.
10. Pull-out tests on corroded high-strength concrete specimens showed more brittle behaviour (sharp decrease in bond strength-slip curve occurred at the peak bond strength values as shown in Fig. 15(b)) compared with its uncorroded condition.
11. The degradation of bond strength in the higher-strength concrete was more pronounced than in the lower-strength concrete. The underlying mechanism of this again was the cause of expansion of the corrosion products as explained above in conclusion number 7.
12. In the case of the uncorroded specimens, the slippage of reinforcement bars decreased with increasing c/D ratio and concrete strength.
13. In the case of the corroded specimens, the slip displacement was less for the lower-strength concrete at the lowest c/D ratio.
14. When the c/D ratio was increased in the case of the corroded specimens, the slip displacement was less for the higher-strength concrete at the same corrosion level and c/D ratio.

It is expected that the differences in bond strength and slip behaviour for corroded reinforcements with different concrete classes and c/D ratios highlighted in this study may provide guidance for the performance evaluation of existing reinforced concrete buildings, especially in the earthquake-prone regions. Although this study was based on pullout tests with prepared specimens and may therefore not reflect the actual behaviour of reinforced concrete sections under the influence of bending, where both concrete and the reinforcement are in tension, the results and findings of this study are general and may be used directly and as a guide for further studies.

Supplementary materials related to this article can be found online at doi:10.1016/j.cemconres.2012.01.003.

References

[1] L. Chung, S.-H. Cho, J.-H.J. Kim, S.-T. Yi, Correction factor suggestion for ACI development length provisions based on flexural testing of RC slabs with various levels of corroded reinforcing bars, Eng. Struct. 26 (8) (2004) 1013–1026.
[2] J.G. Cabrera, Deterioration of concrete due to reinforcement steel corrosion, Cem. Concr. Compos. 18 (1) (1996) 47–59.
[3] Y. Auyeung, P. Balaguru, L. Chung, Bond behavior of corroded reinforcement bars, ACI Mater. J. 97 (2) (2000) 214–221.
[4] L. Chung, J.-H.J. Kim, S.-T. Yi, Bond strength prediction for reinforced concrete members with highly corroded reinforcing bars, Cem. Concr. Compos. 30 (7) (2008) 603–611.
[5] H.-S. Lee, T. Noguchi, F. Tomosawa, Evaluation of the bond properties between concrete and reinforcement as a function of the degree of reinforcement corrosion, Cem. Concr. Res. 32 (8) (2002) 1313–1318.
[6] ASTM C234-91a, Standard Test Method for Comparing Concretes on the Basis of the Bond Developed with Reinforcing Steel, American Society for Testing and Materials annual book of standards, , 1991.
[7] ASTM G1-03, Standard Practice for Preparing, Cleaning, and Evaluating Corrosion Test Specimens, American Society for Testing and Materials, 2003.
[8] J.G. Cabrera, T.A.H. Dodd, S.O. Nwaubani, The effect of curing temperature on the chloride ions diffusion of super plasticised cement and fly ash cement pastes, in: C. Maclnnis (Ed.), Proceedings, Durable Concrete in Hot Climate, ACI SP-139, American Concrete Institute, Michigan, 1993, pp. 61–76.
[9] L. Amleh, A. Ghosh, Modeling the effect of corrosion on bond strength at the steel–concrete interface with finite-element analysis, Can. J. Civ. Eng. 33 (2006) 673–682.
[10] J.J. Chang, A study of the bond degradation of rebar due to cathodic protection current, Cem. Concr. Res. 32 (4) (2002) 657–663.
[11] C. Fang, K. Lundgren, L. Chen, C. Zhu, Corrosion influence on bond in reinforced concrete, Cem. Concr. Res. 34 (11) (2004) 2159–2167.

Fig. 16. Splitting of concrete specimens along the corrosion cracks (see video 2): (a) $w/c = 0.40$; (b) $w/c = 0.75$.Splitting of concrete specimens along the corrosion cracks (see video 2): (a) $w/c = 0.40$; (b) $w/c = 0.75$.